

Role of SMBI deposition in ELM mitigation and the underlying turbulence characteristics

Z. B. Shi¹⁾, Z. C. Yang¹⁾, W. L. Zhong¹⁾, B. Y. Zhang¹⁾, C. Y. Chen¹⁾, M. Jiang¹⁾, P. W. Shi¹⁾, W. Chen¹⁾, Z. T. Liu¹⁾, D. L. Yu¹⁾, Y. Zhou¹⁾, B. B. Feng¹⁾, X. M. Song¹⁾, X. T. Ding¹⁾, Q. W. Yang¹⁾, X. Min¹⁾, and X. R. Duan¹⁾

¹⁾*Southwestern Institute of Physics, P. O. Box 432, Chengdu 610041, China*

Corresponding Authors's e-mail address: shizb@swip.ac.cn

Abstract: The edge localized mode (ELM) mitigation with supersonic molecular beam injection (SMBI) has been studied in the HL-2A H-mode plasmas. The ELM mitigation effect and its relationship with the location of deposited SMBI particle source in the H-mode pedestal are reported experimentally. We found that when the location of SMBI source is about 20% into the pedestal, the distinct ELM mitigation effect is achieved, which is identified by a significant increase of the ELM frequency and also a decrease of the ELM amplitude. A sand-pile model is developed to simulate the ELM burst and explain the mitigation effect for different particle source locations, showing well agreement with the experiments. Both the simulation and the experiment suggest that no deep particle injection is needed for ELM mitigation. The turbulence may play an important role during ELM mitigation. The turbulence grows first, followed by the rapid decrease of the radial electric field. Then the ELM frequency increase, and the sustainment of ELM mitigation is highly correlated with the suppression of inward propagation of turbulence.

1. Introduction

The operation of future magnetic confinement fusion reactors (such as ITER and DEMO), to obtain an energy amplification $Q \gg 1$, is based on the well-established high-confinement mode (H-mode), of which the feature is the reduction of transport near the edge of plasma, leading to steeper gradients of electron and ion temperature as well as density at the region of the so called pedestal [1-2]. In this scenario, the sharp pressure gradient and resulting strong bootstrap current gradient across the edge pedestal area contain substantial free energy that can drive intermittent instabilities with features of quasi-periodic pedestal crash known as edge localized modes (ELMs) [3]. ELM is conducive to the exhaustion of impurity particles from the core plasma, and the dissipation of plasma stored energy, playing an important role in the ELM H-mode operation. Meanwhile, ELMs transport heat and particles from the confinement region across the magnetic separatrix into the open field line region, that may cause a large amount of plasma particle and energy loss, with some concomitant influence, such as damage to the plasma facing components and divertor, bringing of heavy impurities, and weakening of plasma confinement. In the next generation of large device ITER, about 20-40% of the energy losses across the plasma boundary are due to per ELM, and the expected ELM energy will over exceed the wall limit. It has been accepted that the ITER divertor could not endure the energy load due to the natural type-I ELMs, without any action to mitigate [4].

In order to avoid a reduction of the lifetime of the plasma facing components and divertor, energy and particle losses caused by ELMs need to be controlled. The control of ELMs can be achieved either by a complete stabilization of ELMs or by an increase in the ELM frequency [4,5]. The first one is the stabilization of the ELM instabilities, resulting small or no ELMs, such as ELM free H-mode and quiescent H-mode operation [6-8]. The second one is to control energy loss of per ELM with external methods [9-15]. The total ELM energy losses appear to be largely independent of the ELM frequency, an increase in the

frequency leads to smaller loss of per ELM and a reduction in the peak heat loads. Up to now, various approaches have been developed to mitigate the natural ELMs, such as injection of frozen hydrogenic pellets and supersonic molecular beam (SMBI), application of resonance magnetic perturbation (RMP), low hybrid current drive (LHCD), electron cyclotron current drive (ECCD), radio frequency wave (RF), and fast variations ("kicks") of vertical position of the plasma [9-15]. Among them, SMBI is an unique gas injection system based on Laval nozzle technology [16]. It performs better on continuity, penetration depth, and efficiency of fuelling than gas puffing. And the deposition depth of SMBI could be changed manually. This technique has promising potential for fuelling and plasma control application on ITER. A previously published theoretical work [11] suggested that best mitigation is achieved when SMBI deposited to ~ 0.8 of pedestal, close to the outer edge. Recently, a related simulation [17,18] points out that ELM size will be limited within a smaller value when particles deposited to the middle, not the top, of pedestal. This suggests that the way of ELM control with SMBI in the ITER-like large fusion device might be effective, as deep deposition of fuelling injection is hard to achieve with a strong edge transport barrier. And even deposition to the middle needs a powerful injection, which is an advantage of SMBI compared with gas puffing.

The relationship of the mitigation effect and deposition [19], and the characteristic of the turbulence during ELM mitigation are studied experimentally in this work. This paper is arranged as follows. The experimental arrangement and measurement of the pedestal profiles are presented in section II. The feature of ELM mitigation effect is shown in section III. The location of SMBI source deposition is explained in section IV. The ELM mitigation effect with SMBI deposition and sand-pile simulation are described in section V. The features of the turbulence is presented in section VI. The summary and discussion are given in Section VII.

2. Experimental arrangement

The HL-2A device is a medium-sized circular tokamak with the major radius $R_{ax} = 165$ cm, minor radius $a = 40$ cm and a closed divertor, which can be operated in either a limiter configuration or a single null (SN) divertor configuration [20]. The achieved operation parameters are plasma current of I_p

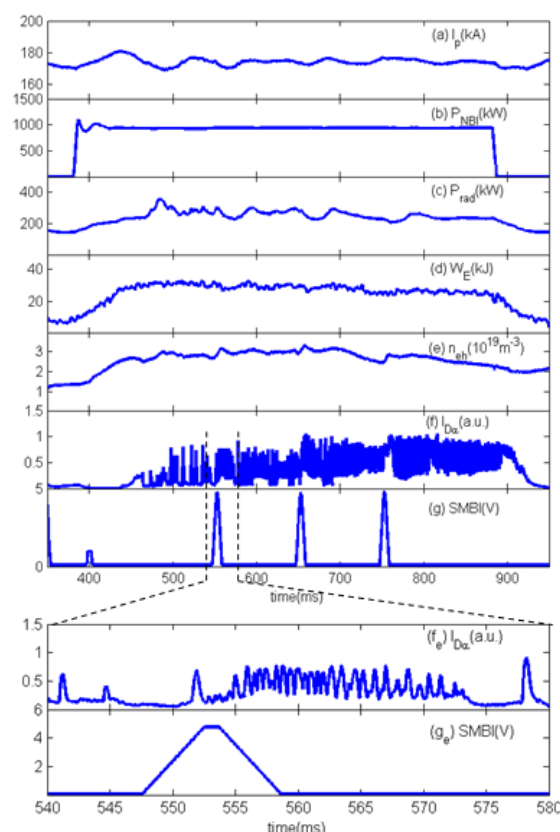


Figure 1: The typical HL-2A H-mode plasma with NBI heating. Temporal evolutions of (a) plasma current, (b) NBI power, (c) plasma radiation power, (d) plasma stored energy, (e) line averaged electron density, (f) divertor Da signal, (g) SMBI signal, and zoom in plot of (f_e) divertor Da signal and (g_e) SMBI pulse for shot #22194. The evolution of divertor Da signal shows a clear increase in ELM frequency after SMBI pulse.

= 450 kA, toroidal magnetic field of $B_t = 2.7$ T, electron and ion temperature of 5 keV and 2.8 keV, respectively, and a line averaged density of $n_{eh} \sim 8 \times 10^{19} \text{m}^{-3}$. The vessel is covered with the carbon fiber compound (CFC) and is routinely siliconized to decrease the wall recycling. The available auxiliary heating and current drive power includes 2 MW neutral beam injection (NBI) (ion energy: 45 keV), 3 MW electron cyclotron resonance heating (ECRH) (six gyrotrons: 68 GHz) and 1 MW LHCD (two klystrons: 3.7 GHz). In recent experiments, stable and repeatable ELM H-mode plasmas have been achieved in HL-2A with high power auxiliary heating. ELM mitigation experiments have been carried out with SMBI, PI, ECRH and LHCD on HL-2A [9-11, 19-20]. In this experiment, the SMBI with a pulse width of 1–6 ms and an injection pressure of 1.5–2 MPa has been used to mitigate the ELMs. The discharge conditions in the present analysis are as following: toroidal magnetic field $B_t = 1.2$ –1.4 T, plasma current $I_p = 150$ –180 kA, plateau time > 1000 ms, line averaged density $n_{eh} = (1.5$ – $3.5) \times 10^{19} \text{m}^{-3}$, NBI power $P_{NBI} = 0.7$ –1 MW, ECRH power $P_{ECRH} = 0.5$ –1.4 MW, and the plasma stored energy $W_E = 20$ –30 kJ.

Figure 1 shows the waveforms of a typical ELM H-mode plasma with high power NBI heating. The NBI power is about 1000 kW from 380 to 880 ms. The plasma density, stored energy, and plasma radiation increase after the onset of NBI power. The L-H transition is observed at 450 ms. The increase of ELM frequency and decrease of its amplitude are observed after the injection of several SMBI pulses during the H-mode phase. This is a typical ELM mitigation phenomenon with SMBI. As shown in figure 1(f), the fluctuation period of one ELM is about several hundred microseconds. Therefore, the high temporal resolution diagnostic systems are required for measuring variations of the pedestal structures. Among them, the key diagnostic systems for ELM mitigation experiment are the reflectometers for density profile and turbulence measurement. The density profiles are measured by the fast sweep frequency modulated continuous wave (FMCW) reflectometer (Q/V band X-mode reflectometer, the corresponding measured density is about $(0$ – $2.5) \times 10^{19} \text{m}^{-3}$ in the case of $B_t \sim 1.3$ T, and the temporal resolution is about 20 μs) and the 8-channel HCN interferometer. The details of the measurements are given in Refs. [21, 22]. The turbulence, poloidal rotation, and radial electric field are measured by the multi-channel Doppler backscattering reflectometer systems [23,24]. The radial and poloidal correlation of the turbulence can be measured [24]. The electron temperature profiles $T_e(r)$ are measured by a 32-channel microwave superheterodyne radiometer [25].

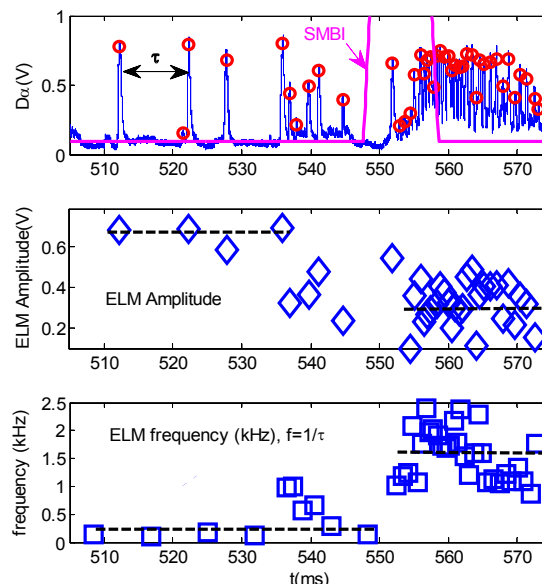


Figure 2: Evolutions of ELM amplitude and ELM frequency during SMBI for shot #22194. (a) divertor D_a and SMBI signals, (b) ELM amplitude, and (c) ELM frequency. The red circles denote the ELM burst peaks. An obvious increase of the ELM frequency and decrease of the ELM amplitude are observed after SMBI.

3. Effect of ELM mitigation with SMBI

Figure 2 shows a typical ELM mitigation effect with a SMBI pulse for shot #22194. An obvious mitigation effect is observed. It can be seen that the burst frequency of ELM on divertor Da signal is increased, but the amplitude and the integral area of each ELM are both decreased after the onset of SMBI pulse. This indicates that the energy attack on the divertor caused by each ELM is reduced.

In order to study the effect of ELM mitigation in different conditions, the frequency and amplitude of ELM is quantified as follows. The ELM frequency is denoted as $f_{\text{ELM}}=1/\tau$, where τ is the time interval between two adjacent ELMs. The averaged values of ELM frequency in a relatively stable state before and after SMBI are denoted as $f_{\text{natural ELM}}$ and $f_{\text{mitigated ELM}}$, respectively. The energy loss caused by one ELM is denoted as the integral area from the baseline to peak of divertor Da signal. Analogous to the clarification of the frequency, the averaged amplitude in a relatively stable state before and after SMBI can be denoted as $E_{\text{natural ELM}}$ and $E_{\text{mitigated ELM}}$. And the same definition also applies for heat flux H_{ELM} , measured by infrared thermography at the divertor. Then the effects of ELM mitigation could be quantified by $f_{\text{mitigated ELM}}/f_{\text{natural ELM}}$ and $E_{\text{mitigated ELM}}/E_{\text{natural ELM}}$. As seen in figure 1 and 2, the increase in ELM frequency of $f_{\text{mitigated ELM}}/f_{\text{natural ELM}}$ is about 4-5, and decrease in ELM amplitude of $E_{\text{mitigated ELM}}/E_{\text{natural ELM}}$ is about 0.5.

4. Location of the SMBI source in pedestal

The particle source deposition of SMBI has been studied by many numerical simulations and experiments [16, 26-28]. Previous studies confirm that SMBI fuelling has the features of higher fuelling efficiency and deeper particle deposition compared with normal gas puffing [16]. It can penetrate into inner region through the last closed flux surface (LCFS). The location of SMBI particle source deposition may play a very important role for ELM mitigation.

There are several methods to estimate the location of particle source deposition: (1) one is the maximum of the Da intensity after SMBI injection, (2) the second one is observation of the electron density pulse propagation. Since SMBI is a kind of particle fueling, the plasma density will increase after the onset of SMBI pulse. At the location of particle source, the density will greatly increase, and then spreads out both inward and outward. The density behavior can be described by particle diffusive equation [29]

$$\frac{dn_e}{dt} = -\nabla \cdot \Gamma + S_p \quad (1)$$

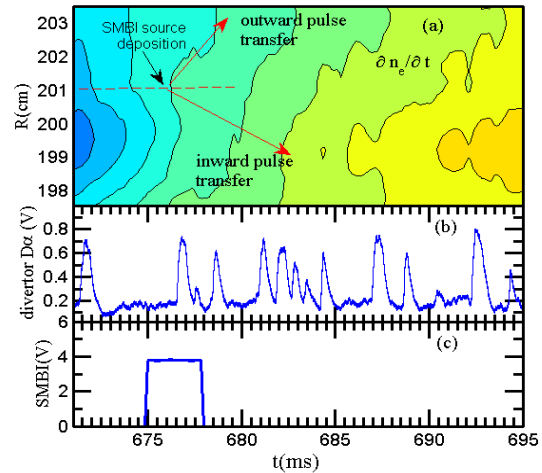


Figure 3: Temporal evolutions of (a) 2D contour plot of the electron density increment ($dn_e(r)/dt$) at different radii, (b) divertor Da signal and (c) SMBI pulse signal for shot #27249. The deposition of SMBI source should be the radial position of the first density increment ($R \sim 201$ cm at $t \sim 676$ ms). The inward and outward pulse transfer from the SMBI source deposition is observed.

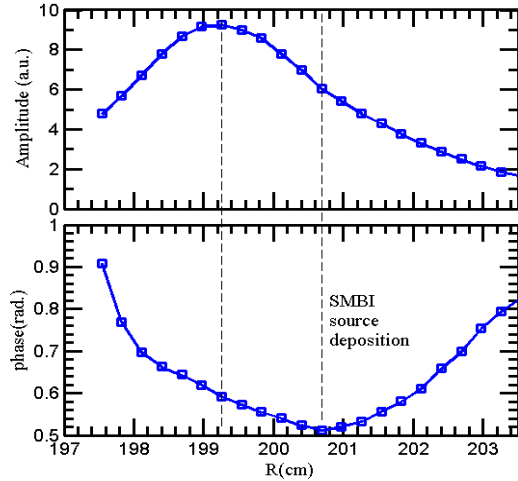


Figure 4: Radial profile of the amplitude and the phase of the first harmonic of Fourier transform of the SMBI modulated density during ELM H-mode for shot #27249. The minimum phase position at about $R = 200.8$ cm denotes the SMBI source deposition. The inward shifted maximum amplitude position indicates a strong inward particle pinch around the source region.

where, S_p is the particle source. The particle flux Γ is determined by particle diffusivity D and the particle pinch V , as $\Gamma = D\nabla n - nV$. In the SMBI modulation experiment, the location of particle source can be obtained from minimum phase of the first harmonic of Fourier transform of the modulated density.

Usually, the lifetime of the particle source is equivalent to the ionization time of SMBI particles, which is much shorter than the diffusive time. As a result, the particle flux can be neglected in the particle diffusive equation right after the onset of SMBI pulse, and the particle diffusive equation can be rewritten as $dn_e/dt = S_p$. At the location of SMBI particle source, the density increment is the most significant response, and the time derivative of the density ($dn_e(r)/dt$) in this region should be greater than that at the other radial position. This can be considered as the direct method to estimate the location of SMBI source deposition. Therefore, the initial radial location of the maximum increase of the local plasma density corresponds to the location of the particle source deposition. The inward and outward density pulse transfer from this location can be observed. Figure 3 shows an example of the location of the SMBI source (shot #27249). The control signal of SMBI starts at $t = 675$ ms. As there is a process of gas flow and ionization, the plasma density starts to increase about 1~2 ms after onset of the SMBI control signal. A local maximum density increment is observed at $R = 201$ cm ($t = 677$ ms). Then, the inward and outward pulse transfer from the SMBI source location is observed, and the line-averaged density starts to increase, which is caused by the ionization of the SMBI source. This source position can be further confirmed by the Fourier

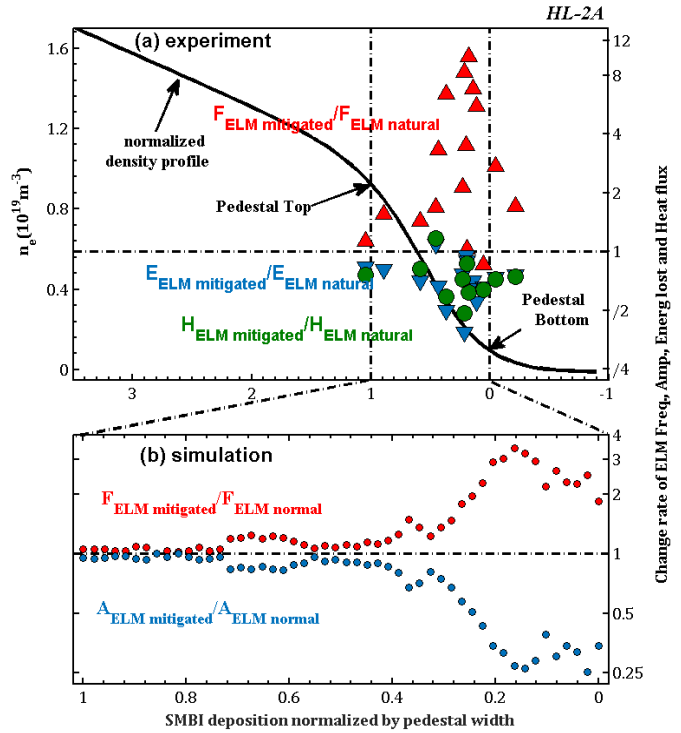


Figure 5: Ratio of ELM frequency and amplitude changed with different SMBI depositions. (a) experimental statistics of the dependence of ELM mitigation effect on SMBI deposition. The electron density profile of edge plasma for general view (line), and ratio of frequency, energy lost, and heat flux changed during SMBI. (b) simulation of ELM mitigation effects with sand pile model.

transform analysis of the modulated density. Figure 4 shows the radial profile of the amplitude and phase of the first harmonic of the SMBI modulated density during ELM H-mode for shot #27249. The minimum phase position at about $R = 200.8$ cm denotes the SMBI source deposition, which is similar with that observed in figure 3. Usually, there is a strong particle pinch around the particle source. Due to the inward particle pinch inside the SMBI source location, the maximum of the amplitude is shifted inward relative to the location of the minimum of the phase.

5. Role of SMBI deposition on the effect of ELM mitigation

Statistical results of the relationship between the SMBI deposition and the effect of ELM mitigation are shown in figure 5 (a). The parameters of pedestal are highly related to the qualities of the H-mode, which is determined by the auxiliary heating, wall recycling, magnetic configuration, and plasma control, etc. In this experiment, the electron density of the pedestal top is about $(0.85-1.2) \times 10^{19} \text{ m}^{-3}$. The width of the pedestal varies in the range of 3.1–4.5 cm. To compare the deposited depth in the pedestal, the x-axis in figure 5 is normalized by width of the pedestal. The bottom and top of the pedestal are defined as 0 and 1, respectively. Most particle sources are deposited within the pedestal region. Based on the mitigation effect defined in section 3, the relationship between ELM mitigation and SMBI deposition position is clearly shown. If the particle source is deposited in the bottom, especially outside of the pedestal, the ELM mitigation is hardly observed. When it injects deeper, deposited about 20% into the pedestal, the distinct mitigation effect is achieved. In this condition, frequency of ELM could grow nearly tenfold; meanwhile, the energy loss could reduce to one third, as well as the heat flux at the divertor. But when the particle source injects further into the middle or deeper region, the mitigation effect degrades rapidly, till frequency and energy loss of ELM did not change obviously, just similar with the condition of bottom deposition.

The one-dimensional self-organized criticality (SOC) sand-pile model [30] is developed to simulate the ELM burst and explain the mitigation effect at different SMBI deposition. It is deemed that there is a threshold to trigger ELMs from the peeling-ballooning mode theory. Since the electron temperature pedestal is not very evident, the electron density profile, instead of pressure, is used in this simulation. When the gradient exceeds the threshold, sand (physical quantities: heat flux or particles) will flow. Since the localized flow will change the gradient around until the gradient is under the threshold everywhere, a local or global crash of the sand-pile might be triggered. In addition, a main source and sink, which represent gain and loss of energy or particles, are set on the top and bottom, respectively. Naturally, the lost quantity of sand through the sink amounts to be the size of ELM. The main source, sink, and threshold of SOC are set up, and the SMBI source will be attached to different positions of the profile. As the experimental interests focuses on the location of particle source, the particle source is simplified to be a point described only by position and size. The position is easy to understand. And the size depends on the main source which is set on the top. It should be smaller than the latter one to lead to ELM behavior that is similar to the experiment, and greater than a critical value to achieve better ELM mitigation effect.

Mitigation effect in simulation with the same definition as the experiment is shown in figure 5 (b), and similar trends can be observed. A clear mitigation is achieved when the particles deposit ~20% of width into the pedestal, that agrees well with the experiment. The

shallower injection deposition makes the crash smaller and more frequent, because it triggers the crash in advance. With the deposition further to the pedestal top, the mitigation effect degrades gradually, which agrees with the experiment well. This may suggest that one or a combined of many physical quantities of pedestal played a role as the threshold, and further lead the response of plasma for SMBI is similar to the automata mechanism in the sand-pile model.

6. Characteristic of turbulence during ELM mitigation

The relevant theoretical works^[31,32] point out that the occurrence of ELM crashes does not only depend on the linear threshold, but also relies on nonlinear processes. The inward propagation of turbulence is found to be an important factor, for a condition to reduce the energy loss of ELM. The perturbation of electron density measured by multichannel Doppler reflectometer is used to analyze the feature of turbulence spreading during ELM mitigation with SMBI. The dispersion relation of the turbulence can be obtained by cross correlation analysis.

$$S(k, \omega) = \langle |P_{xy}(\omega)| \delta(k_{xy}(\omega) - k) \rangle \quad (2)$$

where P_{xy} is the cross power spectrum between two time series $x(t)$ and $y(t)$, $k_{xy}(\omega) = \phi_{xy}(\omega)/d$ is the wave-number, $\phi_{xy}(\omega)$ is the cross phase and d is the distance between two detectors. The summed k spectrum can be obtained as: $S(k) = \sum_{\omega} S(k, \omega)$. Figure 6 shows

the temporal evolutions of wave number spectra in one discharge with several SMBI pulses (shot #24996). The inward spreading of turbulence is observed during the unmitigated phase. The inward spreading diminished and even reversed for the conditions of ELM mitigated or spontaneous high frequency ELM ($f_{\text{ELM}} \sim 1.5$ kHz), although their deposition locations and mitigation effects are different. An inward transmission is observed only in case of low ELM frequency, while in the case of high ELM frequency, the transmission is weak.

Figure 7 shows the trajectory plots in phase space of the ELM frequency and density fluctuation with the radial electric field at pedestal. After SMBI injection, the density fluctuation grows first, followed by the rapid decrease of the radial electric field. This result is similar with that observed in the type-Y limit cycle oscillation [33]. When the density fluctuation is higher than a threshold, the density fluctuation dramatically increases follow by rapid increase of the ELM frequency and decrease of ELM amplitude. This may be caused by

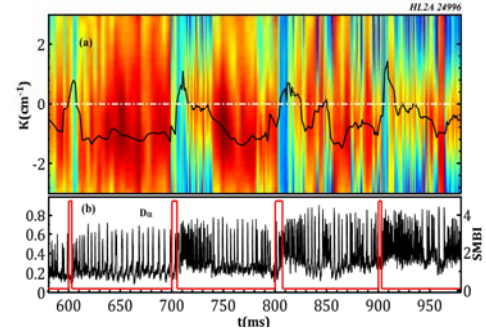


Figure 6: Temporal evolutions of (a) radial wave number spectrum of turbulence in color map, and the peaks highlighted in black line, (b) Da intensity and SMBI signal.

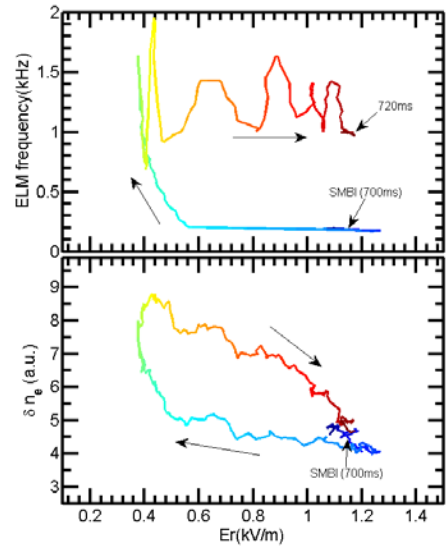


Figure 7: Trajectories plots in phase space of (a) ELM frequency and (b) density fluctuation with the radial electric field (E_r). The color line denotes time trace of the plot.

the neoclassical poloidal flow damping, which is dominated by collisionality [34]. Then, the density fluctuation gradually decreases with the recovery of the radial electric field. The suppression of ELM is kept for several tens milliseconds, until appearance of the inward propagation of the turbulence. This suggests that the sustainment of ELM mitigation is highly correlated with the suppression of inward propagation of the turbulence.

7. Summary and discussion

In this work, role of the location of the SMBI particle source during ELM mitigation is obtained experimentally. The one-dimensional SOC sand-pile model based on the measured density profile is developed to simulate the ELM mitigation effect, showing well agreement the experimental observation. The turbulence plays an important role for ELM mitigation. The increase of turbulence and drop of the radial electric field are observed prior to the ELM mitigation, and the sustainment of ELM mitigation is highly correlated with the suppression of inward propagation of the turbulence.

The measured density profile around the pedestal is used in the simulation. Here we assume that the current density and pressure gradient (drive peeling and ballooning mode and are generally considered caused ELM) and other parameters (e.g., gradient of density and temperature) of the pedestal are similarly distributed, which have a maximum value near the middle of the pedestal. And it has been found that when the threshold has the features described earlier, a simulation result consistent with experiment could be observed. This may suggest that one or a combination of many physical quantities of the pedestal played a role as the threshold, and further lead the response of plasma for SMBI is similar to the automata mechanism in the sand-pile model.

ACKNOWLEDGMENTS

This work is supported by the Chinese National Fusion Project for ITER (2013GB107002, 2013GB104002, 2014GB107001), the National Natural Science Foundation of China (11475057, 11261140326, and 11305053).

References:

- [1] A. W. Leonard, *Physics of Plasmas* 21, 090501 (2014)
- [2] A. E. Hubbard, *Plasma Phys. Control. Fusion* 42, A51 (2000)
- [3] ASDEX Team and F. Wagner, *Phys. Rev. Lett.* 49, 1408 (1982).
- [4] P.T. Lang, et. al., *Nucl. Fusion* 53, 043004(2013)
- [5] G. T. A. Huijsmans, et. al., *Physics of Plasmas*, 22, 021805 (2015)
- [6] L D Horton, et. al., *Plasma Phys. Control. Fusion* 44, A273 (2002)
- [7] Burrell K.H. et al., *Plasma Phys. Control. Fusion* 44, A253 (2002)
- [8] W.L. Zhong, et. al., *Nucl. Fusion* 53, 083030 (2013)
- [9] M.Xu et al., overview of H-2A experiment, IAEA FEC 2016
- [10] Y. Huang, et. al., *Nucl. Fusion* 52, 114008 (2012)
- [11] W.W. Xiao, et. al., *Nucl. Fusion* 52, 114027 (2012)
- [12] X. J. Zhang, et. al., *Phys. Plasmas* 21(6), 061501 (2014).
- [13] B. Gui, et. al., *Phys. Plasmas* 21(11), 112302 (2014).
- [14] Snyder P.B. et al., *Nucl. Fusion* 47, 961 (2007)
- [15] A.W.Degeling, *Plasma Phys. Control. Fusion* 45, 1637 (2003).
- [16] D. L. Yu, et. al., *Nucl. Fusion* 50(03), 035009 (2010).
- [17] S. Y. Chen, et. al., *Physics of Plasmas* 21, 112512 (2014)
- [18] J. Huang, et. al., *Physics of Plasmas* 22, 122507 (2015);
- [19] Z. C. Yang, et. al., *Physics of Plasmas* 23, 012515 (2016)
- [20] X. R. Duan, et. al., *Nucl. Fusion* 53(10), 104009 (2013).
- [21] W. L. Zhong, et. al., *Rev. Sci. Instrum.* 85(1), 013507 (2014).
- [22] Y. Zhou, et. al., *Rev. Sci. Instrum.* 78, 113503 (2007).
- [23] W L Zhong,etal, *Plasma Phys. Control. Fusion* 58, 065001 (2016)
- [24] W.L. Zhong, et. al., *Nucl. Fusion* 55, 113005(2015)
- [25] Z. B. Shi, et. al., *Rev. Sci. Instrum.* 85, 023510 (2014)
- [26] Z.H. Wang, et. al., *Nucl. Fusion* 54, 043019(2014)
- [27] Y. L. Zhou, et. al., *Phys. Plasmas* 22, 012503 (2015)
- [28] Yu-Lin Zhou, et. al., *Chin. Phys. B* 25, 095201 (2016)
- [29] W. W. Xiao, et. al., *Rev. Sci. Instrum.* 81, 013506 (2010)
- [30] T. Rhee, et. al., *Phys. Plasmas* 19(2), 022505 (2012).
- [31] P.W. Xi et al, *Physics of Plasmas*, 21, 056110 (2014)
- [32] C.H.Ma et al, *Physics of Plasmas*, 22, 055903 (2015)
- [33] J. Cheng, et. al., *Phys. Rev. Lett.* 110, 265002 (2013)
- [34] K. C. Shaing, et al., *Phys. Rev. Lett.* 63, 2369 (1989)